

# Mechanical properties and microstructural features of AISI 4340 high-strength alloy steel under quenched and tempered conditions

Woei-Shyan Lee \*, Tzay-Tian Su

*Department of Mechanical Engineering, National Cheng Kung University, Tainan 701, Taiwan*

Received 29 August 1997

## Abstract

In this work, the mechanical properties and microstructures of AISI 4340 high strength alloy steel under different tempering conditions are investigated. The specimens are quenched and tempered to a martensite structure and loaded to fracture at a constant strain-rate of  $3.3 \times 10^{-4} \text{ s}^{-1}$  by means of a dynamic material testing machine (MTS 810). The mechanical properties and strain-hardening exponent are considered as function of the tempering conditions. The morphological features of the as-quenched martensite and their evolution during tempering are described. Fractographs of the specimens are also made in order to analyse their fracture and embrittlement mechanisms. The results indicate that the mechanical properties and microstructural features are affected significantly by tempering temperature and holding time. The strength and hardness of tempered martensite drop as the tempering temperature and holding time are increased. However, the ductility increases with increasing tempering temperature and holding time, except when tempered martensite embrittlement occurs. Microstructural observations reveal that the carbide precipitates have a plate-like structure at low temperatures, but are spheroid-like at high temperatures. Under the tested conditions, the fracture appearances show that the material failed in a ductile manner except for the case of tempering at 300°C, where tempering martensite embrittlement occurs due to the existence of retained interlath austenite. © 1999 Elsevier Science S.A. All rights reserved.

*Keywords:* AISI 4340; High-strength alloy steel; Tempering

## 1. Introduction

An understanding of the mechanical properties of metals during deformation over a wide range of loading conditions is of considerable importance for a number of engineering applications. When discussing high strength steel, it is crucial to realise that the definition of so-called high strength depends entirely upon how the steel is to be used. These usages tend to fall into a number of different categories where different combinations of properties are required. In each of these categories, works being carried out to develop higher strength steels have to take the manufacturing processes, the heat treatment and the alloying technology into consideration [1].

There are several well-known structures in steel, such as ferrite/pearlite, bainite, martensite and austenite. Each of them has very different mechanical properties [2–4]. Therefore, it is possible to obtain the highest strength from any one of these structures and it is likely that the highest strength steel in each of these categories will be of wide application. Generally, quenching and tempering are well-established means to produce strengthening in steel which can be achieved mainly due to the precipitation of a fine dispersion of alloy carbides during tempering [5]. Known for forming the highest level of strength in a steel, the martensite structure is rarely used in an untempered condition because a large number of internal stresses associated with the transformation cause the material to be lacking in ductility [6–8], however, low-temperature tempering is sufficient to reduce these stresses considerably without essentially changing the basic features of the martensitic structure.

\* Fax: + 886 6 2352973; e-mail: wslee@mail.ncku.edu.tw

Table 1  
Chemical analysis of AISI 4340 alloy steel

Elements	C	Si	Mn	Ni	Cr	Mo	P	S
wt.(%)	0.39	0.24	0.61	1.46	0.67	0.17	0.021	0.006

Therefore, from the commercial point of view, the study of martensitic steels have to include that of steels tempered in the range of 200–250°C.

However, apart from the effect of tempering temperature, the strength of the martensitic structure is dominated by the carbon content and the ( $M_s$ – $M_f$ ) temperature range [9,10]. In the case of low-carbon martensite, the martensite units form in the shape of lath, grouped into larger sheaves or packets. Its sub-structure consists of high densities of dislocations arranged in cells, and is superficially similar to that developed in iron by a heavy cold-working process. In the case of high-carbon steels and iron alloys with  $M_s$  below the ambient, their structure is plate martensite, which consists of very fine twins with a spacing of about 50 Å. Their crystal structure may be either (bct) or (bcc). However, in the case of medium-carbon steels, since they may contain a mixture of lath and plate martensite, their structure is more complicated. These results also indicate that the mechanical behaviour of a quenched-and-tempered steel depends strongly on its microstructure. Thus, the study of effects of the microstructure and dislocation structure of a steel on its strength, ductility and fracture characteristics is of great importance from the viewpoint of both theory and practice.

Although AISI 4340 steel is a widely-used low-alloy martensitic steel that provides an advantageous combination of strength, ductility and toughness for the applications of machine part-members, it is susceptible to embrittlement during the tempering procedure within a specified temperature range. In order to prevent this fault, a study on the microstructure and mechanical properties of AISI 4340 steel under different tempering conditions becomes necessary, these questions being focused on in this study. Further, the behaviour of tempered embrittlement as well as its formation mechanisms are also described.

## 2. Material and experimental details

AISI 4340 high-strength alloy steel, supplied in the form of an extruded bar of 25.4 mm diameter, is used in this study, its chemical composition being given in Table 1. AISI 4340 steel is a low-alloy martensitic steel that can be heat treated to provide a wide range of hardness values. Other studies have shown that most of the inclusions in AISI 4340 steel are MnS particles [11].

However, their concentration is reduced considerably by the vacuum arc remelt (VAR) process [12]. For the present tests, in order to obtain different quenched-and-tempered martensite structures, samples from the as-received steel are firstly austenitised at 850°C for 30 min, followed by oil cooling to produce a quenched martensite structure, and then tempered at 100, 200, 250, 300, 400, 500 and 650°C, for 2 and 48 h, respectively. After heat treatment, cylindrical tensile specimens are machined in the longitudinal orientation from the extruded bar. The size and geometry of the specimens as well as the testing procedure are in accordance with ASTM standard E 8 (1981) for tension testing. Under this standard a nominal gauge length of 50 mm and a gauge of 12.5 mm are utilised in preparing the specimens.

For mechanical tests, the specimens are mounted on a dynamic material testing system (MTS) and pulled to fracture at room temperature with a constant cross-head speed of 0.0083 mm s<sup>-1</sup>, which corresponds to an initial strain rate of  $3.3 \times 10^{-4}$  s<sup>-1</sup> (if all the crosshead movement is transmitted to the specimen), in order to obtain the room temperature flow properties. A strain-gage extensometer with a nominal gauge length of 25 mm is utilised to measure the deformation of the specimens and the cross-head motion relative to the central pull-bar. The mechanical properties, such as ultimate tensile strength, yield strength, and percentage reduction area, are calculated from the stress–strain diagrams obtained from the tensile testing, in which the latter three specimens under identical conditions are used.

After mechanical testing, the specimens for transmission electron microscopy (TEM) observation are cut from the fractured tensile halves by a spark cutting machine, first into slices of approximate 0.25 mm thickness, and second into discs of 3 mm diameter. The 3-mm discs are then ground with no. 600 emery paper to thickness appropriate for jet thinning and afterwards electropolished with a jet thinning instrument (Tenupol 3, Struers, double jets) in solution of 5% perchloric acid and 95% acetic acid (by volume) maintained at 0°C with a voltage of 20–30 V, until the discs are perforated. Jet thinning is carried out on both faces of the discs to reduce their thickness at the centre. To prevent the perforation from being damaged by force of the jet, jet thinning has to be discontinued when the samples are nearly perforated, then a window technique is used to perforate these samples delicately. The thin foil specimens are then examined with a Jeol 2000FX elec-

Table 2  
The mechanical properties of AISI 4340 alloy steel after 2 h tempering

Tempering temperature (°C)	100	200	250	300	400	500	650	Quenching
$\sigma_y$ (MPa)	1828	1627	1528	1436	1300	1110	814	2015
$\sigma_T$ (MPa)	1997	1792	1696	1587	1437	1294	977	2214
Hv (62.5 kg)	617	536	497	486	460	407	356	660
A (%)	40	41	42	35	45	50	57.4	33.7
$\varepsilon$ (%)	8.4	8.6	9.8	8.8	10	14	18.1	4.5
$n$	0.53	0.5	0.48	0.42	0.38	0.32	0.21	0.57

tron microscope operating at 200 kV to reveal the dislocation substructure and the precipitation of carbides.

Following the mechanical testing, the observations of the fracture surface for each fractured tensile specimen are also conducted. Sections of the fracture surface are removed from the fractured tensile bar and then treated with standard metallographic procedures for microscopic examination. The observation of the topographical features is carried out using a Jeol JX A-840 scanning electron microscope operated at 2.5 kV.

### 3. Results and discussion

#### 3.1. Effects of tempering temperature and holding time on the mechanical properties

The mechanical properties, i.e. ultimate and yield strengths, hardness, reduction in area, elongation, and strain-hardening exponent  $n$ , are measured as functions of tempering temperature and holding time. For every measurement, three specimens are used, having been quenched (850°C/30 min) in oil and tempered at 100, 200, 250, 300, 400, 500 and 650°C, for 2 and 48 h, respectively. The results obtained are listed in Tables 2 and 3, in which the data for the as-quenched condition are included for comparison. As expected, the mechanical behaviour of AISI 4340 steel is quite sensitive to the tempering temperature and holding time. Under as-quenched conditions, the material has the highest level of strength and hardness, but its ductility is the lowest. This can be explained based on the phase transformation of steel during quenching processes, where the lattice structure of steel changes immediately from a face-centred cubic ( $\gamma$  phase) to a body-centred tetragonal (martensite). At the same time, a large amount of distortion occurred during the formation of the platelets of martensite, which leads to rapid increase of strength and hardness.

For the tempering case, the variations of strength and hardness of the AISI 4340 steel with tempering temperature and holding time are shown in Figs. 1 and 2, and indicate that the strength and hardness decrease as the tempering temperature and holding time are

increased, however, the effect of tempering temperature is more significant than that of holding time. Fig. 3 shows that tested samples' area reduction and elongation varied with the tempering temperature and holding time. It is clear that the ductility of material increases with the tempering temperature and holding time, but that there is then a drop in toughness and ductility when tempered at 300°C.

It has been known for many years that high strength martensitic steel heat-treated to achieve the optimum combination of strength, ductility and toughness may result primarily from different processes of heat tempering. This loss in toughness may result primarily from different processes of heat treatment. Actually, in the as-quenched state, the thermal instability of interlath austenite after tempering often leads to the formation of carbide films, which is a fairly general cause of tempered martensite embrittlement. As for the present case, a loss in toughness after tempering at 300°C is correlated with the retained interlath austenite and the formation of interlath carbide films that are decomposed from the lath boundary retained austenite. The phenomena and possible mechanisms of embrittlement will be described in detail hereinafter in Section 3.3.

#### 3.2. Measurement of the strain-hardening exponent

The true stress–strain curves for AISI 4340 steel conform closely to Ludwik's relationship  $\sigma = K\varepsilon^n$ , where  $K$  is the strength coefficient and  $n$  is the strain-hardening exponent. These two constants describe completely the shape of the true stress–strain curves. The value of ' $K$ ' provides some indication of the level of strength of the material and of the magnitude of forces required in forming, whilst the value of ' $n$ ' correlates the slope of the true stress–strain curve, i.e. the rate of work hardening, which provides a measure of the ability of the material to retard localization of deformation. In uniaxial tension, the equivalent stress  $\sigma_i$  equals the tensile stress  $\sigma$ , and the equivalent strain  $\varepsilon_i$  equals the tensile strain  $\varepsilon$ , consequently the true stress–strain curve is the same as the curve  $\sigma = K\varepsilon^n$ . The stress  $\sigma$  must not be greater than the tensile instability stress  $\sigma_{crit}$  which corresponds to the maximum load in simple tension and in turn marks the end of uniform straining, thus  $\sigma_{crit} = K(\varepsilon_{crit})^n$ .

Table 3  
The mechanical properties of AISI 4340 alloy steel after 48 h tempering

Tempering temperature (°C)	100	200	250	300	400	500	650	Quenching
$\sigma_y$ (MPa)	1778	1557	1450	1367	1237	1037	600	2015
$\sigma_T$ (MPa)	1940	1677	1564	1497	1366	1172	699	2214
Hv (62.5 kg)	597	512	470	457	430	379	660	660
A (%)	44	48	50	44	50	52	33.7	33.7
$\epsilon$ (%)	9.8	9.8	11	9.7	11.5	12.5	4.5	4.5
$n$	0.5	0.44	0.40	0.36	0.31	0.23	0.57	0.57

When the ultimate tensile stress is exceeded, deformation becomes localised to the necked region of the specimen and the material within this region is no longer subject to a purely uniaxial tensile stress but a complicated system of triaxial tensile with shear stress, in which the maximum stress occurs at the centre of the necked region. This phenomenon has been described in detail by Wigley [13]. According to the definition of the strain-hardening exponent for pure tension as mentioned above, the values of  $n$  are determined and summarised in Tables 2 and 3, from which it can be found that the value of  $n$  decreases rapidly with increase of the tempering temperature for both cases of 2 and 48 h, and that the values of the strain-hardening exponent  $n$  are shown to be a linear function of the yield strength, as shown in Fig. 4. This result indicates that under all the present conditions, the deformation of the AISI 4340 steel is dominated by the mechanism, i.e. a thermally activated mechanism, and that the rate of dislocation annihilation is also the same for each increment of tempering temperature. Hollomon and Zener [14] indicate that in a wide variety of steels the product of the yield stress and strain-hardening exponent is found to be a constant,  $\phi$ , having a value in the range of 8000–16000 psi (79–158 MPa). Rosenfield and Hahn [15] made a similar analysis by incorporating their results of line-pipe steel with those of other studies in

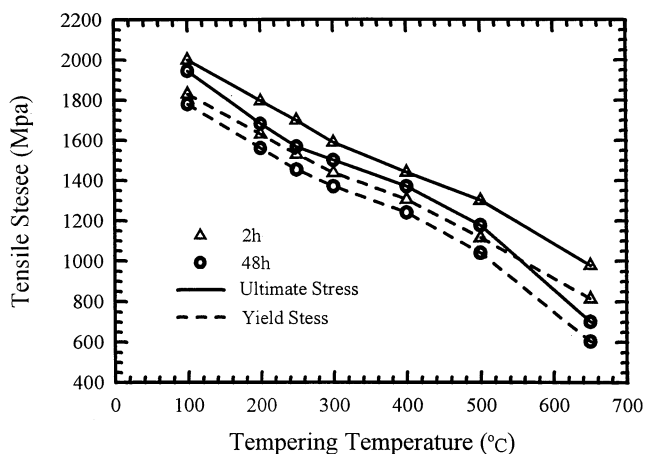


Fig. 1. Variation of ultimate tensile stress and yield stress as a function of tempering temperature for 2 h ( $\Delta$ ), and 48 h ( $\circ$ ).

which the very high strength maraging steels are included. Rosenfield and Hahn's data not only confirm the general conclusion of Hollomon and Zener [14] but also show that a linear relationship exists between the yield stress and the strain-hardening exponent, which demonstrated that for the properties of steel a high strength cannot coexist with high work hardening. Therefore, it is not easy to obtain both a high strength and a high rate of work hardening in the same class of steel.

### 3.3. The effects of tempering temperature and holding time on the fracture behaviour and embrittlement mechanisms

Microscopic observations were made at the fracture surface to help to identify quantitatively the mode of fracture initiation as a function of tempering temperature. For all of the specimens tested, the observation of the fracture surface shows that heavy necking has taken place during tensile loading. The typical ductile 'cup-and-cone' fracture surface includes three parts: the fibre region in the centre; the outside smaller shear lip; and the larger radial region between the two. An example of these features is shown in Fig. 5, which corresponds to that for specimens tempered at 100°C. It should be noted here that, in the as-quenched condition, although some voids appear on the fracture surface, the frac-

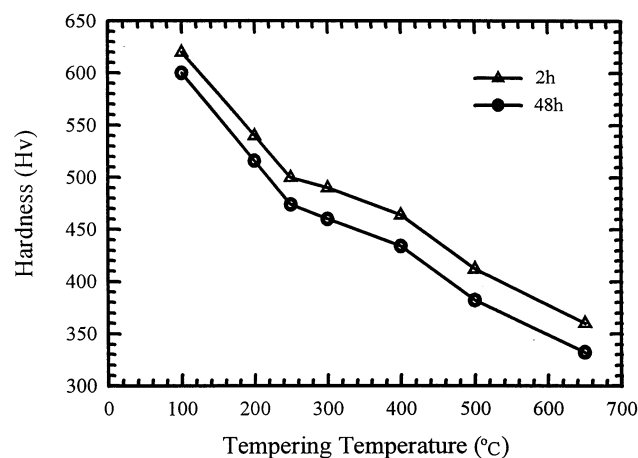


Fig. 2. As for Fig. 1, but for hardness.

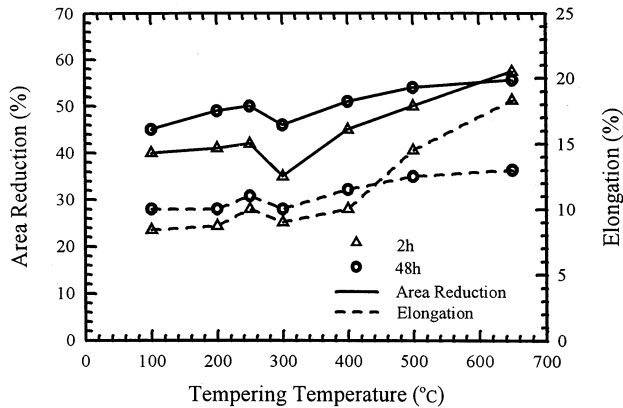


Fig. 3. As for Fig. 1, but for reduction in area and elongation.

tures generally show a low energy cleavage pattern corresponding to a brittle fracture mode (Fig. 6).

For all of the tempered specimens, their fracture characteristic is dominated by the ductile mechanism. Figs. 7 and 8 show the fracture surface of the specimens tempered at 200°C for 2 and 48 h, respectively. The features observed on these micrographs are typical of most of the fracture surfaces for all the tempering temperatures except for the case of 300°C, which is in lack of evidence for toughness. The fine distribution of voids or 'dimples' in Figs. 7 and 8 shows that the tempered AISI 4340 steel failed with a ductile fracture mode. The voids in these micrographs exhibit a fairly wide variation in size and shape. The elongated shape of some voids may indicate that localised shear stresses also occur in addition to tensile stresses, during deformation. It is also noticeable that many of the larger

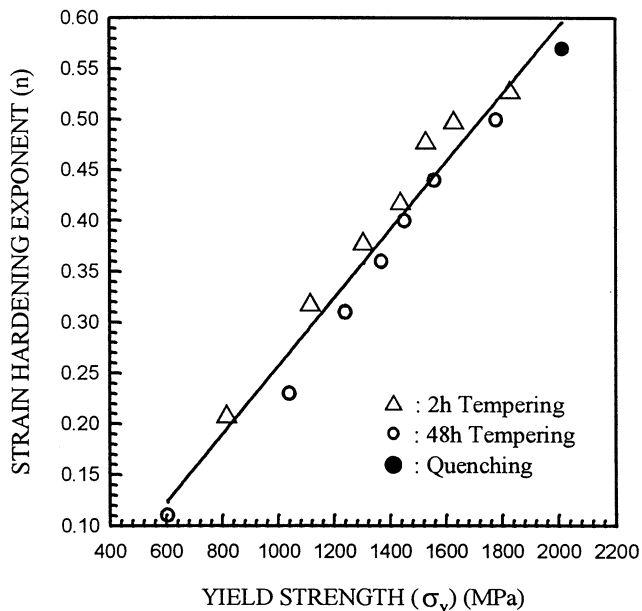


Fig. 4. Effect of the yield stress on the strain-hardening exponent of AISI 4340 steel.

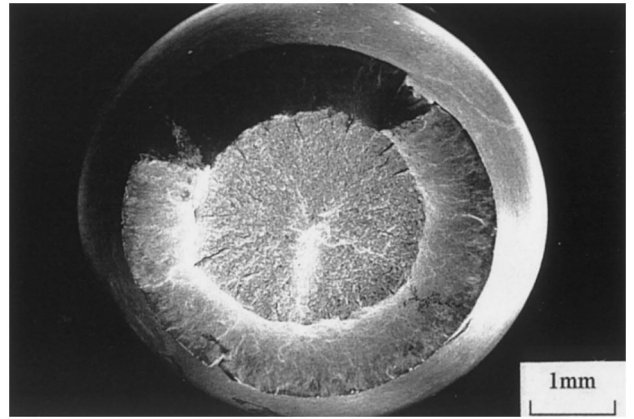


Fig. 5. Fracture appearance of a specimen quenched in oil (850°C/30 min) and tempered at 100°C for 2 h.

voids presented are actually composed of many smaller, shallow voids.

The fractographs of specimens tempered at 300°C are shown in Fig. 9 from which the aforesaid tempered martensite embrittlement occurred. There are two regions which can be clearly distinguished from the fracture appearance: one where the material fractured by cleavage (label A), and the other where it failed by microvoid growth and coalescence (label B). The feature of fracture surface in Fig. 9 also indicates that the amount of brittle fracture in the 300°C tempered condition is greater than that in the other tempered conditions, and that the embrittlement is accompanied by a change in fracture mode from mainly transgranular microvoid coalescence to predominantly intergranular separation along prior austenite grain boundaries.

It is clear that tempered martensite embrittlement in steel can not be generally attributed to a single mechanism. In our test, the austenite is retained as interlath films or discrete blocks in the structure tempered at 300°C. This can be clearly seen in the dark field image (Fig. 10) in which many retained austenite films exist at

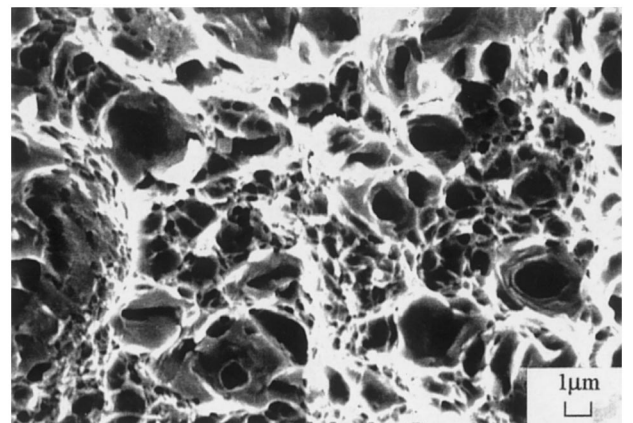


Fig. 6. Fractograph of an AISI 4340 steel specimen, as quenched in oil (850°C/30 min).

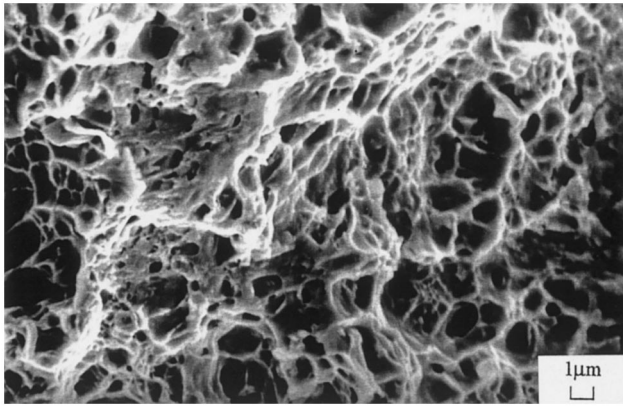


Fig. 7. Fractograph of specimen quenched in oil (850°C/30 min) and tempered at 200°C for 2 h.

the lath boundary. The orientation relationship between  $\alpha$ -ferrite and retained austenite satisfies the K–S relation. Therefore, we can conclude that the lath boundary retained austenite decomposes to form carbide films cementite should be responsible for the tempered martensite embrittlement of AISI 4340 steel under presented testing condition.

When specimens were tempered at the higher temperature of 650°C (Fig. 11), although their fracture features slightly differ from that observed in the lower tempered conditions ( $\leq 500^\circ\text{C}$ ), their fracture mode is still dominated by the transgranular microvoid coalescence. In this condition, the appearance of the fracture surface consists of two types of dimples. The larger ones may result from carbide precipitates and the smaller ones are ascribed to characteristics of the material.

#### 3.4. The variations of microstructure with tempering temperature and holding time

Thin foils of this martensitic steel are studied in detail with TEM to realise the nature of the structural

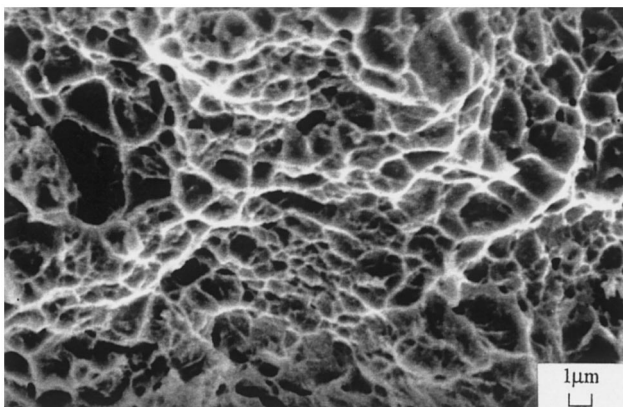


Fig. 8. Fractograph of specimen quenched in oil (850°C/30 min) and tempered at 200°C for 48 h.

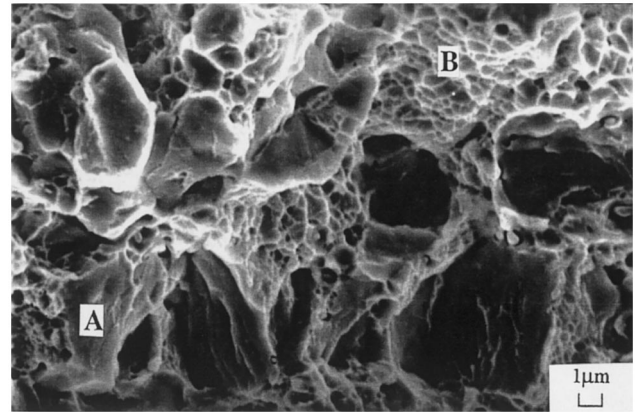


Fig. 9. Fractograph of specimen quenched in oil (850°C/30 min) and tempered at 300°C for 2 h.

changes and the dislocation distribution under the various tempering processes employed.

#### 3.4.1. Structure of the as-quenched martensite of AISI 4340 steel

The morphology of martensites (Fig. 12 (optical microscope) and Fig. 13 (electron transmission microscope)), consists mostly of dislocated martensite laths. Isolated examples of internal twins are also seen in a few plates. Generally, the laths, about 0.5 microns wide, are separated by low angle boundaries and each martensite lath is composed of many dislocation cells.

Since  $M_s$  of AISI 4340 steel is above room temperature, this leads to an autotempering behaviour in the as-quenched structure, thus in the case of quenched martensite there are some brief periods in which carbon atoms can redistribute themselves. Because the stress fields in lath martensite are situated around individual dislocations and cell walls, certain interstitial lattice sites near to these places, seen as defected ones, provide lower energy for carbon than the normal sites. Such migration can be detected by metallography or by a smaller contribution of carbon to electrical resistivity or to internal friction, if comparing the carbon situated in an interstitial site near to a dislocation with that in a 'normal' one [16]. Autotempered precipitates are not present in any of the twinned plates but are only resolved in the dislocated laths and untwinned plates. This suggests strongly that dislocated laths and untwinned plates form first near to  $M_s$ , whilst twinned plates forms at lower temperatures, i.e. near to  $M_f$ .

#### 3.4.2. Quenched and tempered structure of AISI 4340 steel

Tempering, a process of heating the martensite to elevated temperatures for the material to become more ductile, involves many different basic processes, such as: the precipitation of carbides, the decomposition of retained austenite, and the recovery and recrystallisation

tion of martensite structure. In the present cases, when the material is tempered at 200°C for 2 h,  $\epsilon$  carbide ( $\text{Fe}_{2,3}\text{C}$ , hcp) being the carbide precipitated at this temperature. This result confirms totally that of Jack [17], but differs from that of Hirotsu et al. [18], who found that for martensitic high-carbon steel, the carbide precipitated during the first stage of tempering is  $\eta$ -carbide or  $\eta\text{-Fe}_2\text{C}$ . The material's microstructure at this temperature is shown in Fig. 14, in which the tangles of high density dislocations and smaller dislocation cells are the two main characteristics in the dislocation structures. Also,  $\epsilon$  carbide precipitates can be found at the lath martensite.

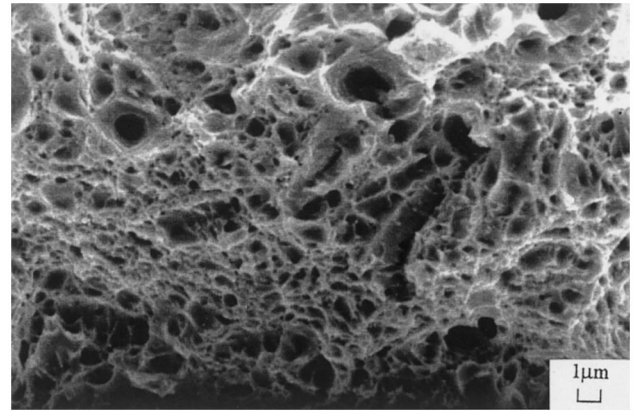


Fig. 11. Fractograph of a specimen quenched in oil (850°C/30 min) and tempered at 650°C for 2 h.

For the case of material tempered at 200°C for 48 h, the observation by TEM shows that some laths grow to larger ones (Fig. 15). Two operating mechanisms should be responsible for the lath growth. One is the movement of lath boundaries and the other is the elimination of lath boundaries due to the movement and annihilation of dislocations at the boundaries. In this tempering condition, high density dislocations with precipitated carbides are present in most of the laths, however, few are invisible. These carbides immobilise the dislocations and cannot form dislocation arrays with a low energy as those at small-angle grain boundaries.

In the case of tempering the martensite of this steel at 300°C for 2 h, dendritic carbide ( $\text{Fe}_3\text{C}$ , orthorhombic) forms and its initial morphology in martensite is plate-like, as shown in Fig. 16. The nucleated site of the carbide is frequently martensite lath boundaries at low temperatures, and ferrite grain boundaries at higher temperatures. For material tempered at 300°C for 48 h, similar dendritic carbide structures are also observed.

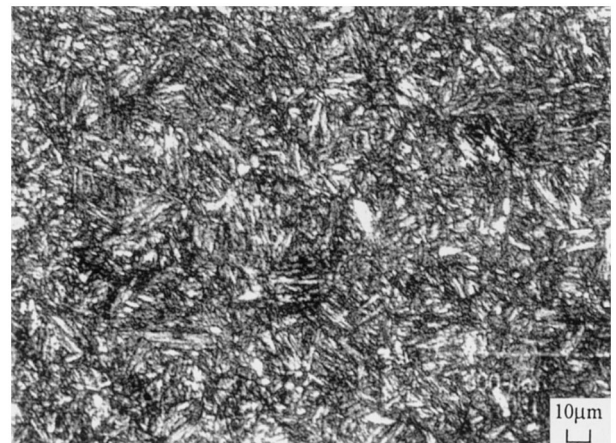
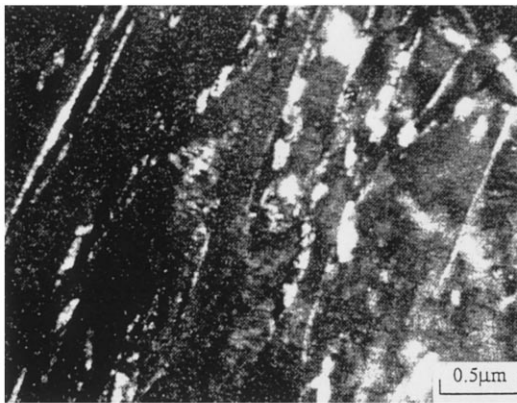


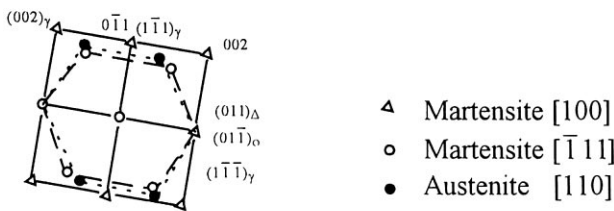
Fig. 12. OM micrograph of the as-quenched martensite of the AISI 4340 steel (quenched in oil, 850°C/30 min).



(a)



(b)



(c)

Fig. 10. Structure of the martensite of AISI 4340 alloy steel tempered at 300°C: (a) DF using one austenite reflection; (b) SADP; and (c) indexing of (b).

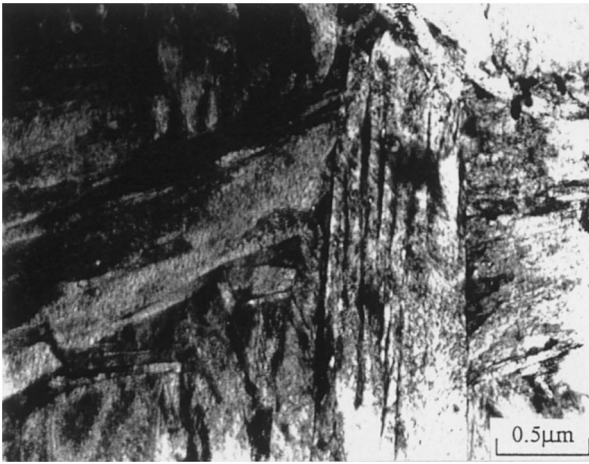


Fig. 13. TEM micrograph of the AISI 4340 steel as-quenched lath martensite.

Growth of the precipitated carbide with tempering holding time can also be seen.

When the quenched structure of AISI 4340 steel is tempered at high temperature, i.e. 650°C for 2 h, the microstructure consists of equiaxed grain of ferrite and different small rod-shaped carbides that distribute within the ferrite matrix in specific directions (Fig. 17). Also, the dislocation cell boundaries and the random dislocations situated between these cell boundaries disappear, whilst a fine cellular structure is developed.

For the case of material tempered at 650°C for 48 h, under such a high temperature and such a long time, the AISI 4340 steel has a ferrite matrix with carbides scattered throughout it (Fig. 18). After recrystallisation is complete, growth of carbide particles and ferrite grain are the only kinetic processes. At this tempering temperature, the occurrence of recrystallisation yields a rapid decrease of the dislocation density and internal strains.

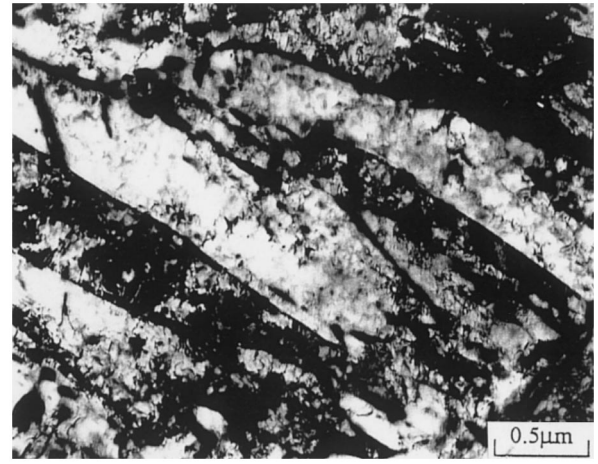


Fig. 15. TEM micrograph of a specimen quenched in oil (850°C/30 min) and tempered at 200°C for 48 h.

tallisation yields a rapid decrease of the dislocation density and internal strains.

It should be noted that when the quenched structure is tempered at high temperature, reaching 650°C, the reaction of  $\text{Fe}_3\text{C}$  to  $\text{Cr}_7\text{C}_3$  takes place, and different types of carbide can be found as shown in Fig. 18. This has been described previously by Lee [19]. Some investigators [20] found that the  $\text{Fe}_3\text{C}$  does not transform directly into  $\text{Cr}_7\text{C}_3$  but actually dissolves in the ferrite matrix whilst the precipitates of  $\text{Cr}_7\text{C}_3$  grow elsewhere. In the present study, the  $\text{Fe}_3\text{C}$  has a needle-like structure at low temperature (Fig. 16), whereas  $\text{Cr}_7\text{C}_3$  (Fig. 18) is in spheroidal form at the high temperature of 650°C. There seems no doubt that  $\text{Fe}_3\text{C}$  formed both a plate-like appearance and a spheroidal form to reduce surface energy. From these results it is tentatively concluded that  $\text{Cr}_7\text{C}_3$  is probably formed due to the reaction of  $\text{Fe}_3\text{C}$  with the matrix.

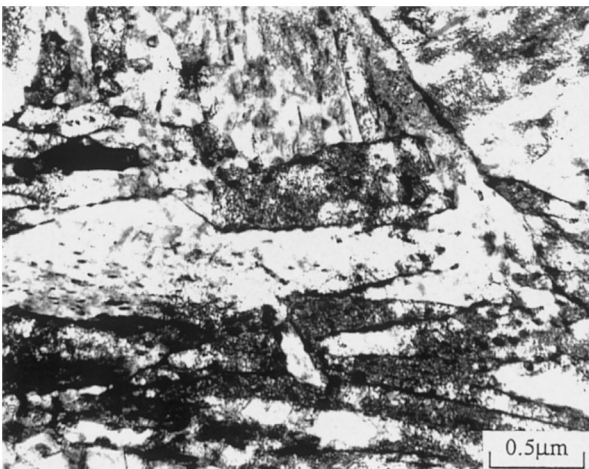


Fig. 14. TEM micrograph of a specimen quenched in oil (850°C/30 min) and tempered at 200°C for 2 h.

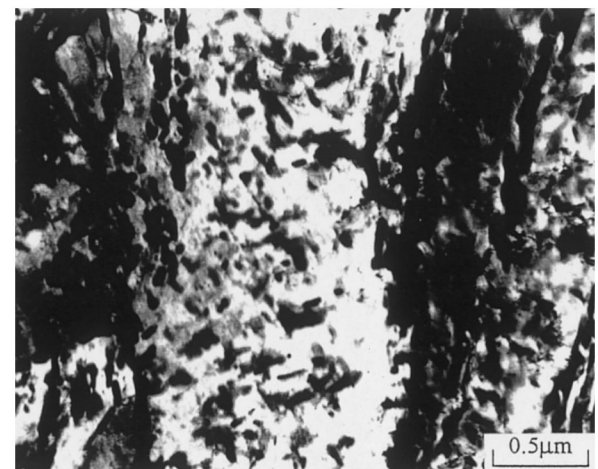


Fig. 16. TEM micrograph of a specimen quenched in oil (850°C/30 min) and tempered at 300°C for 2 h.

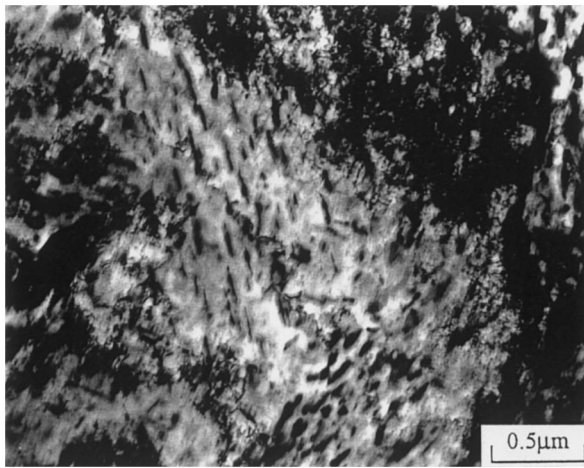


Fig. 17. TEM micrograph of a specimen quenched in oil (850°C/30 min) and tempered at 650°C for 2 h.

#### 4. Conclusions

The mechanical properties and microstructure evolution of AISI 4340 steel under different tempering conditions have been studied. The results from the tensile tests indicate that tempering temperature and the holding time have obvious effects on the mechanical properties and the microstructure features, but the former effect is more pronounced than the latter. Under the tested tempering conditions, the strength, hardness and strain-hardening exponent decrease with an increase in tempering temperature and holding time. It is also found that the area reduction and elongation increase as the tempering temperature and holding time are increased, however, there is a loss in toughness after tempering at 300°C due to retained interlath austenite and the formation of interlath carbide films. TEM observations reveal that the quenched structure within the martensite laths shows extremely high dislocation densities and some microtwins. When tempering at different temperatures, various types of carbide precipitates in different shapes and sizes

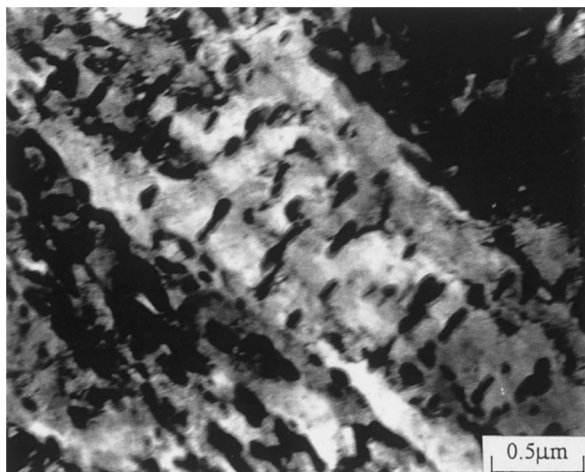


Fig. 18. TEM micrograph of a specimen quenched in oil (850°C/30 min) and tempered at 650°C for 48 h.

appear in the matrix. The distribution of carbides is directly affected by the tempering conditions. At low tempering temperatures, the  $\text{Fe}_3\text{C}$  forms a plate-like structure and is replaced in two stages by  $\text{Cr}_7\text{C}_3$  when the tempering temperature reached 650°C. Fracture analysis shows that for all of the tempering temperatures, the fracture features are predominated by the ductile mode with a dimple structure, except for the case of 300°C, where the material failed in a brittle manner due to the occurrence of tempered martensite embrittlement.

#### References

- [1] K.J. Irvine, The development of high-strength steels, *J. Iron Steel Inst.* 12 (1962) 620–629.
- [2] M.F. Carlson, B.V. Narasimha, G. Thomas, The effect of austenitizing temperature upon the microstructure and mechanical properties of experimental Fe/Cr/C steel, *Metall. Trans.* 10A (1979) 1273–1281.
- [3] M.F. Chai, C. Laird, Mechanisms of cyclic softening and cyclic creep in low carbon steel, *Mater. Sci. Eng.* 93 (1987) 159–174.
- [4] W.D. Callister, *Material Science and Engineering: An Introduction*, 3rd edn, Wiley, New York, 1994.
- [5] D.H. Huang, G. Thomas, Structure and mechanical properties of tempered martensite and lower bainite in Fe–Ni–Mn–C steels, *Metall. Trans.* 2A (1971) 1587–1596.
- [6] C.L. Briant, S.K. Banerji, Tempered martensite embrittlement in phosphorus doped steels, *Metall. Trans.* 10A (1979) 1729–1739.
- [7] H. Kwon, J.C. Cha, C.H. Kim, The effect of grain size on fracture behaviour in tempered martensite embrittlement for AISI 4340 steel, *Mater. Sci. Eng.* 10 (1988) 121–128.
- [8] R.M. Horn, R.O. Ritchi, Mechanisms of tempered martensite embrittlement in low alloy steel, *Metall. Trans.* 9A (1978) 1039–1047.
- [9] K. Shimizu, Z. Nishiyama, Electron microscopic studies of martensitic transformation in iron alloys and steels, *Metall. Trans.* 3A (1972) 1055–1066.
- [10] S.K. Das, G. Thomas, Structure and mechanical properties of Fe–Ni–Co–C steels, *Trans. ASM* 62 (1969) 659–668.
- [11] Y.V. Murty, J.E. Morral, T.Z. Kattamis, R. Mehrabian, Initial coarsening of manganese inclusion, *Metall. Trans.* 6A (1975) 2031–2039.
- [12] C.F. Hickey, A.A. Anticil, Split heat mechanical property comparison of ESR and VAR 4340 steel, *Tech. Report AMMRC TR*, 1983, Brown University, RI, pp. 83–27.
- [13] D.A. Wigley, *Mechanical Properties of Metals at Low Temperatures*, Plenum Press, New York, 1971.
- [14] J.H. Hollomon, C. Zener, Determination of material constant of steel and comparison of results for various constitutive models, *J. Appl. Phys.* 15 (1944) 22–31.
- [15] A.R. Rosenfield, G.T. Hahn, Effect of cold work on mechanical properties of high strength ferrous alloys, *Trans. ASM* 59 (1966) 962–970.
- [16] G.R. Speich, W.C. Leslie, Tempering of steel, *Metall. Trans.* 3A (1972) 1043–1055.
- [17] K.H. Jack, Morphology and crystal structure of carbides precipitated from solid solutions in iron alloys, *J. Iron Steel Inst.* 169 (1951) 26–33.
- [18] Y. Hirotsu, S. Nagakura, Structure and mechanical properties of Fe–Cr–C–Co steel, *Acta Metall.* 20 (1972) 645–655.
- [19] W.S. Lee, T.B. Wu, The influence of tempering conditions on microstructural features of Ni–Cr–Mo steel, in: *Proceedings of the Annual Conference of the Chinese Society for Material Sciences*, April, 1993, pp.11–17–1–24.
- [20] K. Kuo, Carbides in chromium, molybdenum and tungsten steels, *J. Iron Steel Inst.* 4 (1953) 363–373.